

Journal of Materials Chemistry A

Materials for energy and sustainability

Accepted Manuscript

This article can be cited before page numbers have been issued, to do this please use: B. Y. Xia, F. Yang, P. L. Deng, Q. Wang, J. Zhu, Y. Yan, L. Zhou, K. Qi, H. Liu and H. S. Park, *J. Mater. Chem. A*, 2020, DOI: 10.1039/D0TA03565C.



This is an Accepted Manuscript, which has been through the Royal Society of Chemistry peer review process and has been accepted for publication.

Accepted Manuscripts are published online shortly after acceptance, before technical editing, formatting and proof reading. Using this free service, authors can make their results available to the community, in citable form, before we publish the edited article. We will replace this Accepted Manuscript with the edited and formatted Advance Article as soon as it is available.

You can find more information about Accepted Manuscripts in the [Information for Authors](#).

Please note that technical editing may introduce minor changes to the text and/or graphics, which may alter content. The journal's standard [Terms & Conditions](#) and the [Ethical guidelines](#) still apply. In no event shall the Royal Society of Chemistry be held responsible for any errors or omissions in this Accepted Manuscript or any consequences arising from the use of any information it contains.

Metal-organic Framework-derived Cupric Oxide Polycrystalline Nanowires for Fast Carbon Dioxide**Electroreduction to C2 Valuables**View Article Online
DOI: 10.1039/D0TA03565C*Fan Yang^a, PeiLin Deng^a, Qingyong Wang^a, Jiexin Zhu^b, Ya Yan^c, Liang Zhou^b, Kai Qi^a, Hongfang Liu^a,**Ho Seok Park^{d*}, and Bao Yu Xia^{a*}*

^a *Key Laboratory of Material Chemistry for Energy Conversion and Storage (Ministry of Education), Key Laboratory of Material Chemistry and Service Failure, School of Chemistry and Chemical Engineering, Wuhan National Laboratory for Optoelectronics, Huazhong University of Science and Technology (HUST), 1037 Luoyu Road, Wuhan 430074, PR China*

^b *State Key Laboratory of Advanced Technology for Materials Synthesis and Processing, International School of Materials Science and Engineering, Wuhan University of Technology, Wuhan, 430070, PR China*

^c *School of Materials Science and Engineering, University of Shanghai for Science and Technology, 516 Jungong Road, Shanghai, 200093, PR China*

^d *Department of Health Sciences and Technology, Samsung Advanced Institute for Health Sciences and Technology (SAIHST), SKKU Advanced Institute of NanoTechnology (SAINT), School of Chemical Engineering Sungkyunkwan University*

**Corresponding authors: byxia@hust.edu.cn (B.Y. Xia); phs0727@skku.edu (H. S. Park)*

Abstract: Carbon dioxide (CO₂) electroreduction is promising in balancing carbon cycle for sustainable society. However, efficient electrocatalyst is the key to selectively convert CO₂ and generate valuable products.

In this work, metal-organic frameworks (MOFs) derived porous cupric oxide nanowires are prepared by controllable annealing method for the efficient CO₂ reduction. This polycrystalline nanocatalysts demonstrates a high Faradaic efficiency (FE) of ~70% for C₂ products at -1.3 V vs. RHE. A partial current density of ~141 mA cm⁻² for ethylene with a FE of ~37% is achieved in a home-made flow cell at -1.3 V vs. RHE. The in-/ex-situ investigations indicate that the oxide-derived metallic copper with the abundant interfaces would be the real active sites for highly selective CO₂ electrolysis. This work offers effective copper catalysts to selectively convert CO₂ toward valuable products, and more importantly provides insightful understandings in developing efficient catalytic materials for energy conversion.

Keywords: Carbon dioxide reduction; Electrocatalyst; Oxide-derived Cu; Interface; Hydrocarbons;

The growing population and developing industrial lead to the sharp increasing of fossil fuel demand and carbon dioxide (CO₂) emission, which consequently result in the greenhouse effect and ocean acidification.^[1] ^{View Article Online}
^{DOI: 10.1039/C9JA00000A}
² CO₂ conversion is promising to reduce CO₂ emission and balance carbon cycle for the sustainable society.^[3]
Compared to the slow photochemical conversion in nature, the electrochemical CO₂ reduction powered by renewable energy is viable as it can be easily controlled under ambient condition and simultaneously generate valuable products.^[4, 5] However, this process involves the complex multistep electron-coupled-proton reaction, which leads to multiple products and even the hydrogen by-product from the competitive hydrogen evolution reaction (HER).^[6] Among them, C₂ products including ethylene (C₂H₄) are more desirable for the industrial economy and energy fuel application.^[7] Therefore, exploring efficient electrocatalysts to realize CO₂ conversion for generating the target C₂ products is highly desirable.

Among various metallic catalysts, copper compounds are the most promising alternatives for converting CO₂ to hydrocarbons.^[8-10] Consequently, crystalline engineering,^[11, 12] structure designing^[13, 14] and composition tuning approaches^[10, 15, 16] are extensively employed to enhance the activity and selectivity of Cu-based materials in the CO₂ conversion. Nevertheless, their efficiencies in the selective generation of C₂ products are still low due to the competitive HER and other products generated simultaneously during the CO₂ reduction process.^[5] Recently, oxide-derived copper (OD-Cu) polycrystals have been proved to be effective in CO₂ conversion.^[12, 17, 18] For example, the thick Cu₂O films prepared by annealing Cu foil demonstrates a capability in generating a wide product distribution of carbon monoxide, methane, ethylene, etc.^[17] Moreover, Kanan's group reported a high FE of ~50% over the OD-Cu nanoparticles with rich grain boundaries (GBs) for the reduction of CO to ethanol and acetate.^[19] It is believed that the strong binding capability of intermediates (CO*, COH*, CHO*) on the (sub)surface of OD-Cu catalysts is the key to realize the deep CO₂ reduction.^[12, 18, 20] These OD-Cu nanomaterials are the interconnected nanocrystalline network, which endow intrinsically abundant interface, and these metastable sites at the surfaces/interface may be responsible for its

unusual catalytic properties.^[12, 19] Therefore, realizing the controlled synthesis and understanding the structural elucidation of OD-Cu with abundant surface/interface will enable the design of more efficient CO₂ reduction catalysts for the target C2 valuables.^[19, 21]

Metal-organic frameworks (MOFs) are emerged as a new class of porous materials, which are constructed by organic ligands and metal ions with the atomic level periodicity.^[22] Their uniform distribution of metal ions in the MOFs would provide the excellent opportunities to form the polycrystalline with interconnected network and abundant interface.^[23] To this end, we employ the copper-aspartic acid (Cu-ASP) nanofibers to prepare cupric oxide (CuO) nanowires for the CO₂ electrolysis.^[24] As expected, the porous CuO nanowires with abundant crystalline surface/interface are successfully achieved by the controllable annealing treatment. The resultant CuO nanowires exhibit excellent activity for the selective CO₂ reduction with a maximum FE of 70% for C2 products (C₂H₄ and CH₃CH₂OH) at -1.3 V vs. RHE in a H-cell. A smaller onset potential (< -0.3 V vs. RHE) and partial current density of ~141 mA cm⁻² are achieved at -1.3 V vs. RHE for C₂H₄ with FE of ~37% in a home-made flow cell. Moreover, the ex-/in-situ results reveal that the oxide-derived metastable Cu sites at the surface/interface would be active sites for the stabilization of intermediate and the production of C2 valuables. This work provides effective Cu electrocatalysts and significant understandings for selective CO₂ reduction, we anticipate the MOF-derived concept may provide crucial insights in the surface/interface engineering for preparing efficient electrocatalyst toward selective CO₂ conversion technologies.

The porous CuO nanowires are obtained by controllable annealing Cu-ASP nanofibers at 300~600 °C in the air environment. X-ray powder diffraction (XRD) pattern of the initial Cu-ASP materials reveals the well-define MOFs crystalline structure without any Cu or CuO impurities (Figure S1).^[24] The pure CuO phase (JCPDS: 44-0706) is found after annealing process, which suggests the complete oxidation and transformation of Cu-ASP precursors to CuO (Figure S2). Moreover, the annealing process also results in the morphology and structure changes. Scanning electron microscopy (SEM) images show the rougher surface and bigger

nanoparticles with the increase of annealing temperatures (Figure S3). The CuO nanowires obtained by annealing at 400 °C demonstrate the wheat spikes-like morphology with porous structure (Figure 1a), which is significantly different with the smooth surface of initial Cu-ASP nanofibers (Figure S1b). Transmission electron microscopy (TEM) image in Figure 1b clearly shows the porous structure of CuO nanowires, the selected-area electron diffraction (SAED) pattern contains bright rings and spots (Figure 1b inset), indicating the polycrystal nature for CuO nanowires. Closer observation in Figure 1c reveals that these nanoparticles (30-50 nm) are linked in the nanowire form. Moreover, high-resolution (HR) TEM image confirms the interconnected nanocrystal particles (Figure S4). This unique structure contains abundant phase surface/interface, as there are the distinct grain boundary and lattice distortion regions (Figure 1d). HRTEM image verifies the CuO (002) and CuO (111) planes with the lattice spacings of 0.25 nm and 0.23 nm, respectively (Figure 1d inset).

The catalytic activity of CuO nanowires for CO₂ reduction is firstly studied in H-cell system, in which the electrolyte is CO₂-saturated 0.1 M potassium bicarbonate (KHCO₃), and the catalysts are loaded onto the glassy carbon electrode. As the CuO nanowires would be reduced by in-situ electrochemical CO₂ reduction, these samples are denoted as OD-Cu-1~5 respectively. The commercial polycrystalline Cu foil is often used as a reference material for comparison with copper-based materials.^[17] As shown in linear sweep voltammetry (LSV) curves (Figure 2a), the Cu foil and OD-Cu catalysts demonstrate the obvious current density responses in the CO₂-saturated KHCO₃ compared with Ar-saturated KHCO₃ electrolytes (Figure S5). Moreover, the current density response of OD-Cu-3 catalyst is significantly higher than that of Cu foil (Figure 2a), suggesting a possible higher activity of CO₂ reduction for OD-Cu-3 nanowires. The gaseous and liquid products are then analyzed by gas chromatography (GC) and nuclear magnetic resonance (NMR) spectroscopy, respectively. Except the dominated hydrogen product due to the competitive HER, the major reduction products of Cu foil include C1 products such as CO, HCOOH and CH₄, and few C2 products (Figure S6a, S7a). However, MOF-

derived Cu catalysts exhibit enhanced generation in the C2 products. According to the product distribution, the FE of H₂ and C1 products gradually decrease over the OD-Cu catalyst, while the FE of C2 products (C₂H₄ and CH₃CH₂OH) increase under more-negative potentials (Figure S6). In particular, the OD-Cu-3 shows a remarkably high FE of ~70% for C2 hydrocarbons (43% C₂H₄ and 25% CH₃CH₂OH) at -1.3 V vs. RHE (Figure 2b). Furthermore, OD-Cu-3 catalyst also shows a much higher current density of ~20 mA cm⁻² for hydrocarbons at -1.4 V vs. RHE, while the Cu foil shows only ~1.5 mA cm⁻². The partial current densities and FE of OD-Cu catalysts for C2 products are well-overpass Cu foil at the same potential range (Figure 2c), as the C1 and H₂ products have occupied for more than half of total FE of the Cu foil (Figure S7). In addition, the OD-Cu-3 electrode also demonstrates an excellent electrochemical stability. The current density and FE of major product C₂H₄ is remained during the 12 h CO₂ electrolysis at -1.3 V vs. RHE (Figure 2d). Compared with other Cu-based catalysts, this OD-Cu nanowires also show a comparable FE and current density for C2 hydrocarbons (Table S1).^[13, 23, 25-29] However, the partial current density of C₂H₄ is still limited due to the poor solubility of CO₂. In order to overcome the CO₂ mass transport issues, a home-made flow cell equipped with gas-diffusion electrodes (GDEs) is employed. As shown in Figure 2e, the current response is significantly improved, and the onset potential is reduced to < -0.3 V vs. RHE (Figure 2e). The FE of C₂H₄ is ~ 40% and the partial current density is ~105 mA cm⁻² at -1.1 V vs. RHE (Figure 2f). And the partial current density for C₂H₄ can further reach ~141 mA cm⁻² at -1.3 V vs. RHE with a comparable FE of ~37%, which demonstrates the practical potential of this CO₂ electrolysis system. The GDE separates the CO₂ gas and alkaline electrolyte, which reduce the CO₂ diffusion pathway and directly react with CO₂ in gaseous. Thus, compared with the H-cell results, the higher current density and lower onset potential are achieved in the flow cell. Furthermore, the electrochemical double layer capacitance (C_{dl}) determines the electrochemical active area (ECSA) (Figure S8), which represents the number of active sites to some degree. As a result, the OD-Cu-3 provides the highest ECSA and it implies a similar trend in the CO₂ reduction activity (Figure 2c). Therefore, the high CO₂

reduction catalytic activity of series OD-Cu catalysts would be partially ascribed to the active sites created by the controllable annealing treatment. And the intrinsic activity of OD-Cu series catalysts is investigated by ECSA-corrected current density, the similar partial current densities of C2 products indicate the same intrinsic activity among OD-Cu series catalysts (Figure S9).

Since the metal oxides catalysts would also suffer the reduction simultaneously during the cathodic CO₂ electrolysis,^[27, 30] XRD technique is then employed to investigate the phase structure change. As shown in Figure 3a, CuO is totally reduced into metallic Cu (JCPDS: 04-0836) after the CO₂ electrolysis. Moreover, the peak pair of Cu 2p XPS spectrum at 933.5 and 953 eV is attributed to Cu(II), and another couple peaks at ~943 and 962 eV is Cu(II) satellites in CuO nanowires. Whereas, OD-Cu just shows the typical peaks at ~932.5 and 952.3 eV for Cu(0)/Cu(I) species, as the same time, the strong Cu²⁺ satellite peaks in CuO nanowires disappear. It is distinctly different from the Cu(II) states in the initial CuO nanowire before the CO₂ electrolysis (Figure 3b). The Cu LMM Auger spectra in Figure 3c further indicates the different oxidation state in the OD-Cu sample, the presence of Cu(I) and Cu(II) species in OD-Cu are mainly resulted from the inevitable oxidation by exposing to air. Furthermore, the adsorption of OH⁻ on the CuO precursor and OD-Cu sample are then evaluated in 0.1 M KOH at a scan rate of 10 mV s⁻¹ (Figure 3d), as the adsorption of OH⁻ can be used as a substitution for CO₂^{-*},^[31-33] which is a very important intermediate in the CO₂ conversion.^[12, 17, 34] The potential for surface OH⁻ adsorption on CuO precursor is close to that of OD-Cu, but OD-Cu demonstrates a much higher peak intensity than CuO, indicating the similar adsorption affinity yet much more adsorption quantity of OH⁻ on OD-Cu.

Follow the phase changes in the electrochemical CO₂ electrolysis, the morphology evolution of OD-Cu nanowires is then examined (Figure S11). After the electrolysis, the whole nanowires morphologies of OD-Cu are maintained (Figure 4a). TEM image shows the surface of nanoparticles become slightly rougher while the core/shell structure is apparently found (Figure 4b). The SAED pattern of OD-Cu (Figure 4b inset) is

obviously different from the initial CuO nanowires (Figure 1b inset). The clear diffraction rings reveal the emergence of metallic Cu crystalline, which is agreement well with the TEM observations. [View Article Online](#) [Close](#) [Close](#) HRTEM images in Figure 4c and 4d reveals the inter-planar spaces of 0.20 nm, 0.24 nm and 0.27 nm, which are respectively correspond to Cu₂O (111), Cu (111) and Cu (200) facets. Both HRTEM images show some cuprous oxide phase located at the surface and the crystalline Cu phase at the subsurface. Nevertheless, the abundant interface is also remained in the *in-situ* formed OD-Cu materials (Figure S11). TEM images reveal the structural phase evolution of CuO precursor to the metallic phase, while the presence of cuprous oxide phase in OD-Cu surface would be attribute to the inevitable oxidation in contact with air (Figure 3).^[35, 36] The transformation of valence state for element copper are then investigated by *in-situ* Raman spectra during the CO₂ electrolysis (Figure 4e). Before applying an external potential (0 s), the peaks at ~300 and ~620 cm⁻¹ are attributed to the CuO phase. While the peaks attributed to CuO disappear within 180 s of applying potential, which indicates the CuO catalyst would be reduced to the metallic copper quickly. Once the potential is removed, the peaks at ~150, ~300 and ~625 cm⁻¹ are observed and the peak at 150 cm⁻¹ is assigned to Cu₂O. This phenomenon suggests the very active surface of this OD-Cu, which can be oxidized quickly by the oxygenates in the electrolyte. The consequent *in-situ* Raman rounds also evidence the fast *in-situ* reduction and oxidation.

In addition, the aspartic acid organic ligand includes the N element, and the N 1s XPS spectra of CuO and OD-Cu also indicate the existence of N element (Figure S10). In order to exclude the influence of N element on the catalytic result, the aspartic acid is replaced by the succinic acid, which does not contain amino group of N element and only retains other parts. The copper-succinic acid (Cu-SUC) MOFs is prepared and the CuO-SUC is achieved by annealing the Cu-SUC MOFs at 400 °C with 1 h (Figure S12). Similar to the OD-Cu, CuO-SUC shows the porous structure formed by the interconnected nanoparticles. And the corresponding catalytic results are also similar with the OD-Cu catalysts (Figure S13, S6 and S7), which indicates N-doping

does not contribute to the enhanced CO₂ reduction and the controllable annealing treatment on Cu-MOFs is feasible to enhance the selectivity on C₂ products. Moreover, based on the ex-/in-situ results and EISA measurement, we can speculate the real active sites of the series OD-Cu materials would be the active interface/surface at the grain boundary or distortion region. Previous results suggest these abundant metastable sites at the surfaces/interface under the electrochemical reduction environment may be responsible for its unusual catalytic properties.^[12, 19] These active sites at grain boundary/defective regions can stabilize the key *CO and *COH intermediates. These oxide-derived Cu catalysts would possess strong CO-binding capability,^[20, 37, 38] this property could suppresses the reduction of CO₂ to C₁ product and enhances CO₂ hydrogenation to C₂ species via C-C coupling process (the rate-limiting CO* + CO* → OCCO* step or *CO + H* → *CHO step).^[19, 39, 40] Finally, C₂ products will be highly selectively generated on the abundant surfaces/interface of MOF-derived copper oxide catalysts.

In summary, porous CuO nanowires with abundant crystalline surface/interface are successfully achieved by the controllable annealing treatment for selective CO₂ electrolysis. The resultant CuO nanowires exhibit a maximum FE of ~70% for C₂ products (C₂H₄ and CH₃CH₂OH) at -1.3 V vs. RHE. A smaller onset potential (<-0.3 V vs. RHE) and partial current density of ~141 mA cm⁻² are achieved at -1.3 V vs. RHE for C₂H₄ production in a home-made flow cell. The ex-/in-situ results reveal that the abundant surface/interface of the oxide-derived metastable Cu would be beneficial for the stabilization of intermediate and promote the fast production of C₂ valuables. This work provides effective Cu electrocatalysts and significant understandings for selective CO₂ reduction, we anticipate the MOF-derived concept may provide crucial insights in the surface/interface engineering for preparing efficient electrocatalyst toward selective CO₂ conversion.

Conflicts of interest

There are no conflicts to declare.

Acknowledgements

This work is funded by the National Natural Science Foundation of China (21802048, 21805103, 21805104), the Fundamental Research Funds for the Central Universities (2018KFYXKJC044, 2018KFYYXJJ121, 2017KFYXKJC002) and the National 1000 Young Talents Program of China. The authors also acknowledge the support of the Analytical and Testing Center of Huazhong University of Science and Technology for XRD, SEM, TEM, NMR and XPS measurements.

Reference

- [1] J. G. Canadell, C. Le Quéré, M. R. Raupach, C. B. Field, E. T. Buitenhuis, P. Ciais, T. J. Conway, N. P. Gillett, R. Houghton, G. Marland, *Proc. Natl. Acad. Sci.* **2007**, *104*, 18866.
- [2] M. R. Raupach, G. Marland, P. Ciais, C. Le Quéré, J. G. Canadell, G. Klepper, C. B. Field, *Proc. Natl. Acad. Sci.* **2007**, *104*, 10288.
- [3] J. B. Greenblatt, D. J. Miller, J. W. Ager, F. A. Houle, I. D. Sharp, *Joule* **2018**, *2*, 381.
- [4] D. T. Whipple, P. J. Kenis, *J. Phys. Chem. Lett.* **2010**, *1*, 3451.
- [5] D. D. Zhu, J. L. Liu, S. Z. Qiao, *Adv. Mater.* **2016**, *28*, 3423.
- [6] Q. Lu, F. Jiao, *Nano Energy* **2016**, *29*, 439.
- [7] D. Gao, R. M. Arán-Ais, H. S. Jeon, B. R. Cuenya, *Nat. Catal.* **2019**, *2*, 198.
- [8] D. Gao, F. Cai, G. Wang, X. Bao, *Curr. Opin. Green Sus. Chem.* **2017**, *3*, 39.
- [9] S. Nitopi, E. Bertheussen, S. B. Scott, X. Liu, A. K. Engstfeld, S. Horch, B. Seger, I. E. Stephens, K. Chan, C. Hahn, *Chem. Rev.* **2019**, *119*, 7610.
- [10] A. Vasileff, C. Xu, Y. Jiao, Y. Zheng, S.-Z. Qiao, *Chem* **2018**, *4*, 1809.
- [11] A. Loiudice, P. Lobaccaro, E. A. Kamali, T. Thao, B. H. Huang, J. W. Ager, R. Buonsanti, *Angew. Chem. Int. Ed.* **2016**, *55*, 5789.
- [12] C. W. Li, J. Ciston, M. W. Kanan, *Nature* **2014**, *508*, 504.
- [13] M. Ma, K. Djanashvili, W. A. Smith, *Angew. Chem. Int. Ed.* **2016**, *55*, 6680.
- [14] R. Reske, H. Mistry, F. Behafarid, B. Roldan Cuenya, P. Strasser, *J. Am. Chem. Soc.* **2014**, *136*, 6978.
- [15] S. Ma, M. Sadakiyo, M. Heima, R. Luo, R. T. Haasch, J. I. Gold, M. Yamauchi, P. J. Kenis, *J. Am. Chem. Soc.* **2016**, *139*, 47.
- [16] D. Kim, J. Resasco, Y. Yu, A. M. Asiri, P. Yang, *Nat. Commun.* **2014**, *5*, 4948.
- [17] C. W. Li, M. W. Kanan, *J. Am. Chem. Soc.* **2012**, *134*, 7231.
- [18] D. Ren, Y. Deng, A. D. Handoko, C. S. Chen, S. Malkhandi, B. S. Yeo, *ACS Catal.* **2015**, *5*, 2814.
- [19] X. Feng, K. Jiang, S. Fan, M. W. Kanan, *ACS Cent. Sci.* **2016**, *2*, 169.
- [20] Y. Zhou, F. Che, M. Liu, C. Zou, Z. Liang, P. De Luna, H. Yuan, J. Li, Z. Wang, H. Xie, *Nat. Chem.* **2018**, *10*, 974.
- [21] A. Verdager-Casadevall, C. W. Li, T. P. Johansson, S. B. Scott, J. T. McKeown, M. Kumar, I. E. Stephens, M. W. Kanan, I. Chorkendorff, *J. Am. Chem. Soc.* **2015**, *137*, 9808.
- [22] S. L. James, *Chem. Soc. Rev.* **2003**, *32*, 276.
- [23] D.-H. Nam, O. S. Bushuyev, J. Li, P. De Luna, A. Seifitokaldani, C.-T. Dinh, F. P. García de Arquer, Y. Wang, Z. Liang, A. H. Proppe, *J. Am. Chem. Soc.* **2018**, *140*, 11378.

- [24] I. Imaz, M. Rubio-Martínez, W. J. Saletta, D. B. Amabilino, D. Maspoch, *J. Am. Chem. Soc.* **2009**, *131*, 18222.
- [25] H. Zhang, Y. Zhang, Y. Li, S. Ahn, G. T. R. Palmore, J. Fu, A. Peterson, S. Sun, *Nanoscale* **2019**, *11*, 12075. DOI: 10.1039/D0TA03565C
- [26] D. Raciti, K. J. Livi, C. Wang, *Nano Lett.* **2015**, *15*, 6829.
- [27] F. Yang, A. Chen, P. L. Deng, Y. Zhou, Z. Shahid, H. Liu, B. Y. Xia, *Chem. Sci.* **2019**, *10*, 7975.
- [28] X. Tan, C. Yu, C. Zhao, H. Huang, X. Yao, X. Han, W. Guo, S. Cui, H. Huang, J. Qiu, *ACS Appl. Mater. Inter.* **2019**, *11*, 9904.
- [29] C.-W. Kung, C. O. Audu, A. W. Peters, H. Noh, O. K. Farha, J. T. Hupp, *ACS Energy Lett.* **2017**, *2*, 2394.
- [30] P. Deng, H. Wang, R. Qi, J. Zhu, S. Chen, F. Yang, L. Zhou, K. Qi, H. Liu, B. Y. Xia, *ACS Catal.* **2020**, *10*, 743.
- [31] A. Salehi-Khojin, H.-R. M. Jhong, B. A. Rosen, W. Zhu, S. Ma, P. J. Kenis, R. I. Masel, *J. Phys. Chem. C* **2013**, *117*, 1627.
- [32] S. Zhang, P. Kang, T. J. Meyer, *J. Am. Chem. Soc.* **2014**, *136*, 1734.
- [33] F. Lei, W. Liu, Y. Sun, J. Xu, K. Liu, L. Liang, T. Yao, B. Pan, S. Wei, Y. Xie, *Nat. Commun.* **2016**, *7*, 12697.
- [34] S. Gao, Y. Lin, X. Jiao, Y. Sun, Q. Luo, W. Zhang, D. Li, J. Yang, Y. Xie, *Nature* **2016**, *529*, 68.
- [35] P. De Luna, R. Quintero-Bermudez, C.-T. Dinh, M. B. Ross, O. S. Bushuyev, P. Todorović, T. Regier, S. O. Kelley, P. Yang, E. H. Sargent, *Nat. Catal.* **2018**, *1*, 103.
- [36] Y. Lum, J. W. Ager, *Angew. Chem. Int. Ed.* **2018**, *57*, 551.
- [37] K. P. Kuhl, E. R. Cave, D. N. Abram, T. F. Jaramillo, *Energ. Environ. Sci.* **2012**, *5*, 7050.
- [38] H. Mistry, A. S. Varela, C. S. Bonifacio, I. Zegkinoglou, I. Sinev, Y.-W. Choi, K. Kisslinger, E. A. Stach, J. C. Yang, P. Strasser, *Nat. Commun.* **2016**, *7*, 12123.
- [39] J. H. Montoya, C. Shi, K. Chan, J. K. Nørskov, *J. Phys. Chem. Lett.* **2015**, *6*, 2032.
- [40] F. Calle-Vallejo, M. T. M. Koper, *Angew. Chem. Int. Ed.* **2013**, *52*, 7282.

Figure and caption

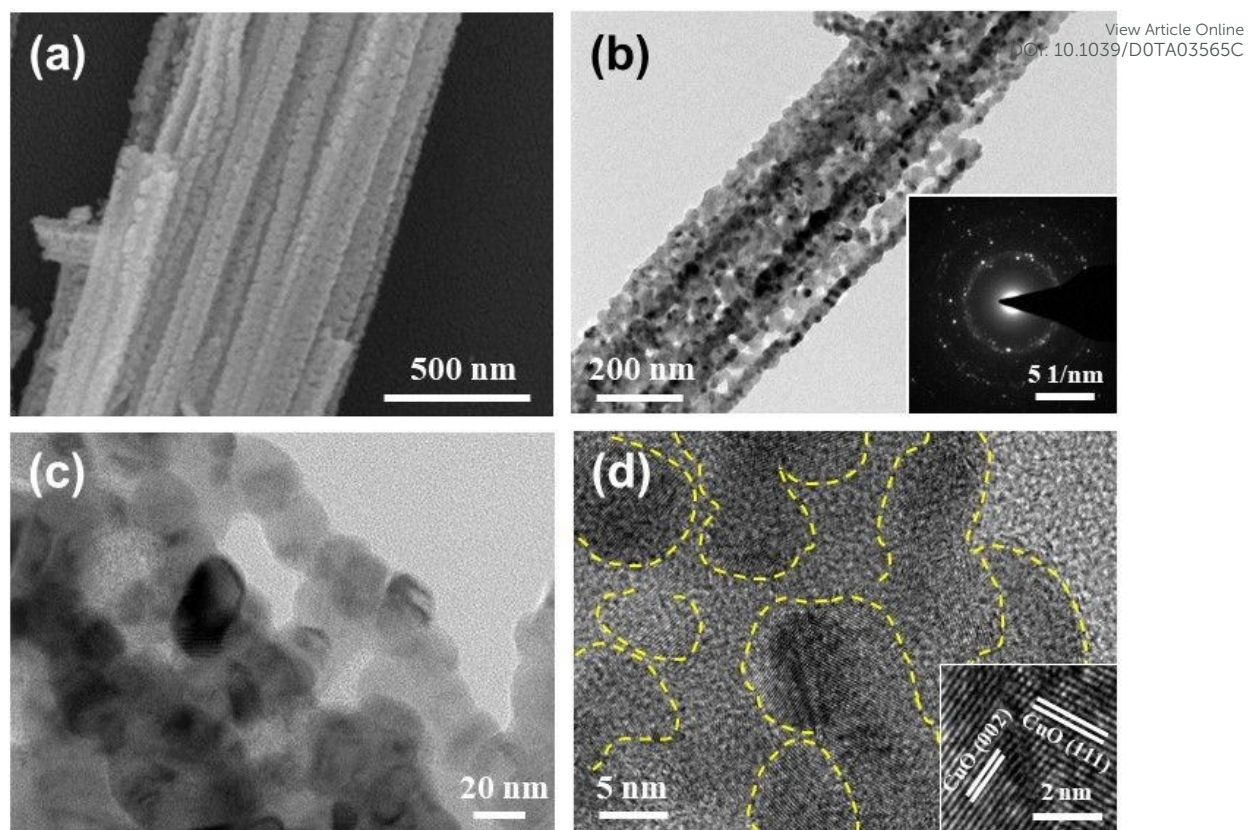


Figure 1. (a) SEM, (b, c) TEM, (d) HRTEM images of CuO nanowires. Inset (b) SAED pattern, inset (d) HRTEM image of lattice fringe.

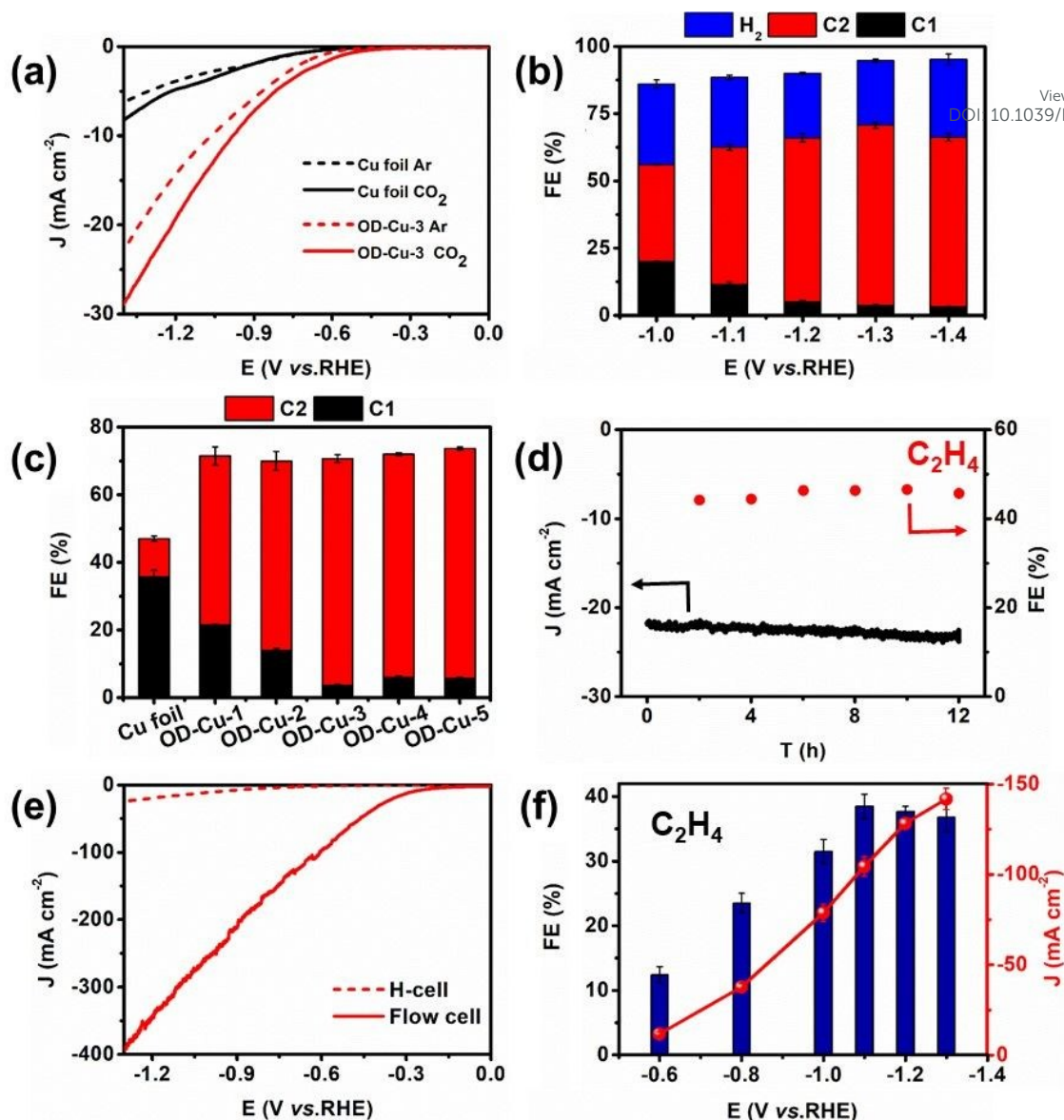


Figure 2. (a) LSV curves of Cu foil and OD-Cu-3 catalyst in Ar-/CO₂-saturated 0.1 M KHCO₃ solution, (b) products FE of OD-Cu-3 at each potential, (c) FE of C₁ (CH₄, HCOOH, CO), C₂ (C₂H₄ and CH₃CH₂OH) products of different catalysts at -1.3 V vs. RHE, (d) Stability test of OD-Cu-3 at -1.3 V vs. RHE during the 12 h electrolysis, (e) LSV curves of OD-Cu-3 in the H-cell and flow cell. (f) FE and partial current density of C₂H₄ (red dots) in the flow cell.

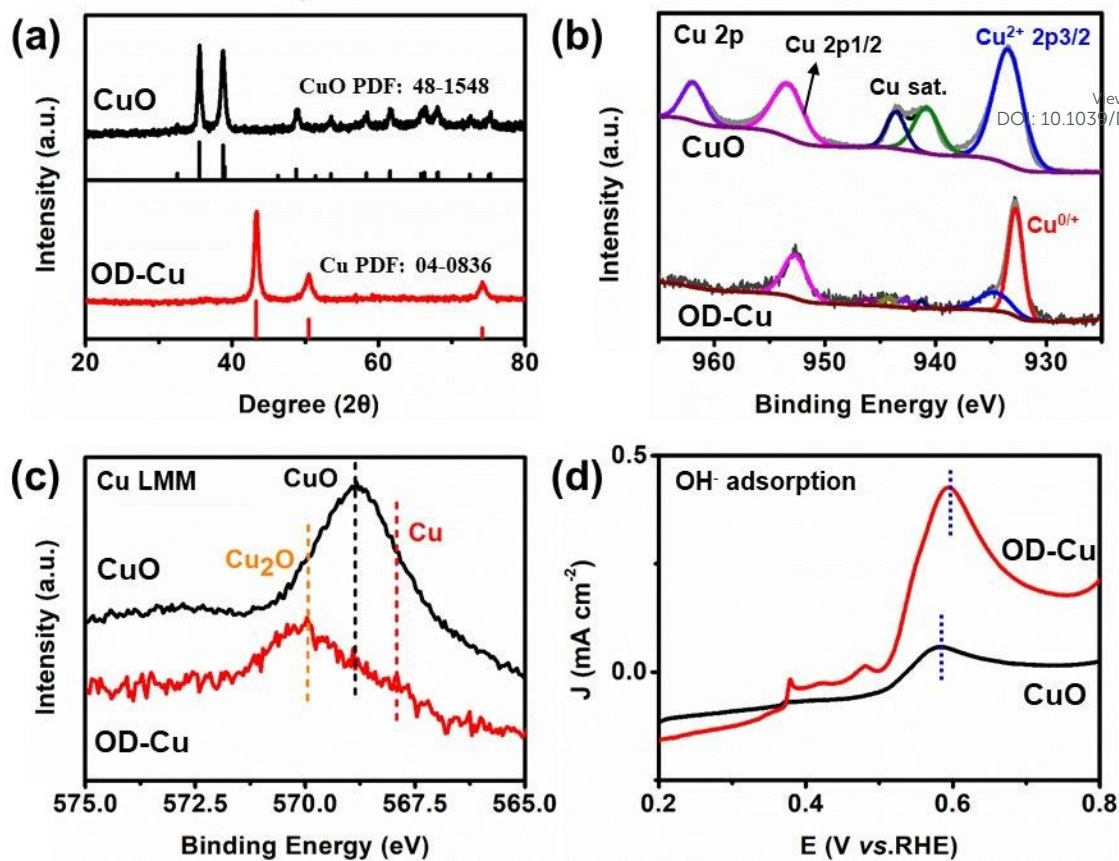


Figure 3. (a) XRD pattern, (b) Cu 2p XPS spectra, (c) Cu LMM Auger spectra, (d) single oxidative scans in 0.1 M KOH at a scan rate of 10 mV s⁻¹ on CuO and OD-Cu catalysts.

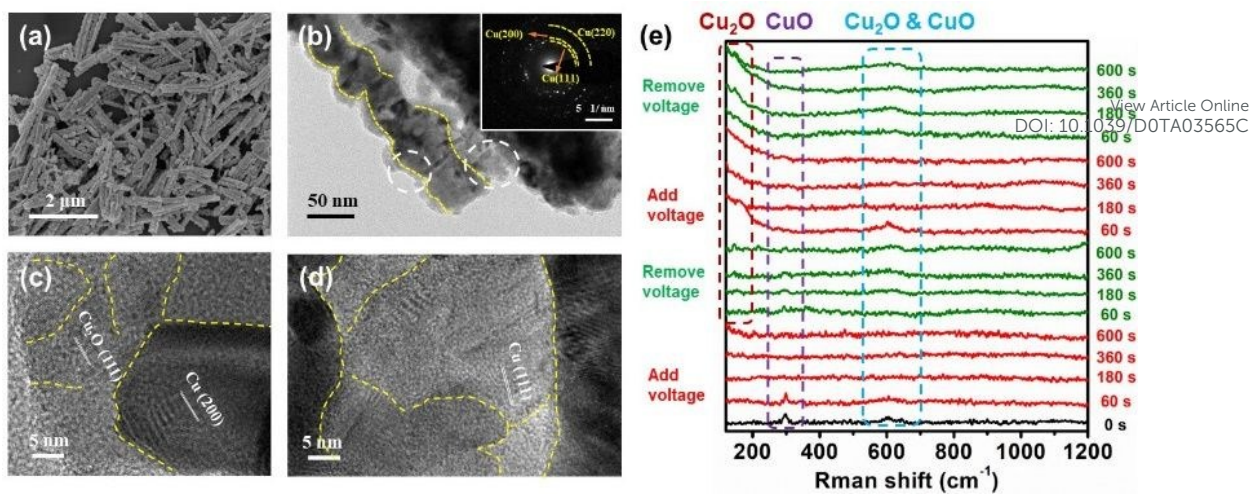
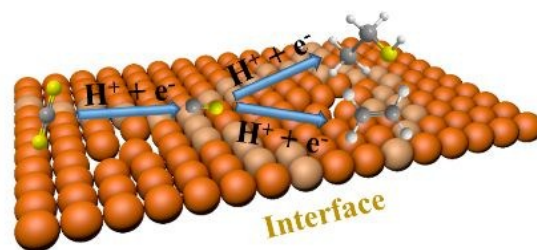


Figure 4. (a) SEM, (b) TEM, (c, d) HRTEM images and (e) in-situ Raman spectra at -1.0 V vs. RHE for OD-Cu-3 catalyst. Inset of (b) is the corresponding SAED pattern.



Enriching Interface: Metal-organic Framework-derived copper oxide nanowires with abundant crystalline interface contribute to the efficient electrochemical CO₂ reduction towards the fast hydrocarbon generation.